

Supporting material:

Oxygen Vacancies Induced Exciton Dissociation of Flexible BiOCl Nanosheets for Effective Photocatalytic CO₂ Conversion

Zhaoyu Ma,^{†1} Penghui Li,^{‡&1} Liqun Ye,^{†‡*} Ying Zhou,^{‡&*} Fengyun Su,[†] Chenghua Ding,[†]
Haiquan Xie,[†] Yang Bai,[‡] Po Keung Wong,[#]

[†] Engineering Technology Research Center of Henan Province for Solar Catalysis; Collaborative Innovation Center of Water Security for Water Source Region of Mid-line of South-to-North Diversion Project of Henan Province; Nanyang Normal University, Nanyang 473061, China.

[‡] State Key Laboratory of Oil and Gas Reservoir Geology and Exploitation, Southwest Petroleum University, Chengdu 610500, China

[&] The Center of New Energy Materials and Technology, School of Materials Science and Engineering, Southwest Petroleum University, Chengdu 610500, China.

[#] School of Life Sciences, The Chinese University of Hong Kong, Shatin, N.T, Hong Kong SAR, China.

***Correspondence author:**

Nanyang Normal University

E-mail: yeliquny@163.com

Southwest Petroleum University

E-mail: yzhou@swpu.edu.cn

¹The authors contributed equally.

1. Experimental

1.1 Synthesis

First, 0.002 mol $\text{Bi}(\text{NO}_3)_3 \cdot 5\text{H}_2\text{O}$ were dissolved into 40 mL glycerol. Then dissolve 0.0015 mol KCl in the previous solution. The suspension was transferred into Teflon-lined stainless steel autoclaves (50 mL), and then the oven was kept at 160 °C for 17 h. After reaction, the complex precursors precipitate was obtained by centrifugation, and then washed with ethanol and distilled water several times. Finally, it was dried at 60 °C in air.

1.2 Characterization

The phase and crystal structure of the photocatalysts were obtained by X-ray diffraction (XRD) on a Bruker D8 diffractometer using Cu K α radiation, the scanning range was from 5° to 65° with the 2 θ scan rate of 6 min⁻¹. Morphology and chemical composition of the samples were analyzed using the Sigma Zeiss Field emission scanning electron microscopy (FESEM) and energy dispersive X-ray spectrometry (EDS) with the accelerating voltage 20KV. The high-resolution transmission electron microscopy (HRTEM) images and element mapping were obtained by a JEOLJEM-2100F (UHR) field emission transmission electron microscopy. UV–vis diffuse reflectance spectroscopy (DRS) of samples were determined by a UV–vis spectrometer (Perkin Elmer, Lambda 850, BaSO₄ as a reference) and record on the within the scope of 200–800nm. X-ray photoelectron spectroscopy (XPS) of samples was characterized by a Thermo Scientific ESCALAB 250XI X-ray photoelectron spectrometer (Al K α , 150 W, C1s 284.8 eV). A Quantachrome Autosorb-IQ automated gas sorption system was utilized to assessing the Brunauer–Emmett–Teller (BET) surface areas at 77K. Time-resolved PL spectra (340 nm excitation) recorded by a FLS980 Multifunction Steady State and Transient State Fluorescence Spectrometer (Edinburgh Instruments, room temperature). Transient absorption spectra recorded at 365 nm by a NTA Transient State absorption Spectrometer (Beijing Perfect light Technology Co., Ltd., China).

1.3 Photocatalytic reduction of CO₂

The photocatalytic reduction activities for CO₂ conversion was done in Labsolar-III AG (Beijing Perfect light Technology Co., Ltd., China) closed gas system. The volume of the reaction system was 350 mL and 1.3 g NaHCO₃ was added firstly. Then 0.05g photocatalyst in the ultrasonic cleaning apparatus dissolved in an appropriate amount of water, then the resulting suspension transfer on a watch-glass with an area of 28.26 cm² paving, the watch-glass is then placed in a vacuum drying oven at a temperature of 60 degrees. About 30 minutes of drying, the photocatalyst becomes very thin film completely covered in glass, and then the watch-glass was put in mid-air of the reaction cell. Prior to the light irradiation, the above system was thoroughly vacuum-treated to remove the air completely, and then 10 mL 4 M H₂SO₄ was injected into the reactor to react with NaHCO₃. Then, 1 atm CO₂ gas was achieved. After that, the reactor was irradiated from the top by a 300 W high pressure xenon lamp (PLS-SXE300, Beijing Perfect light Technology Co., Ltd., China), and the photoreaction temperature was kept at 20 C by DC-0506 low-temperature thermostat bath (Shanghai Sunny Hengping Scientific Instrument Co., Ltd., China). During the irradiation, 1 mL of gas was taken from the reaction cell for subsequent qualitative analysis by GC9790II gas chromatography (GC, Zhejiang Fuli Analytical Instrument Co., Ltd., China) equipped with a flame ionization detector (FID, GDX-01 columns). The quantification of the production yield was based on a calibration curve. The outlet gases were determined to be CO, CH₄ and CO₂.

1.4 Light to carbon monoxide (LTCO) conversion efficiency calculations

The “light -to-carbon monoxide” conversion efficiency (LTCO) was determined to be: $LTCO = E_F/E_{light} = (\text{energy of CO}_2 \text{ conversion into CO and O}_2)/(\text{light energy irradiating the reaction cell})$.

The light energy conversion was evaluated by using 300 W Xenon lamp as the light source 1 h of illumination, the surface was about 4 cm²

$$UV\text{-Vis: } 0.57W \text{ cm}^{-2}$$

$$\text{So, } E_{light} = T * W = 3600 * W \text{ J.}$$

E_F was the energy generated by CO₂ conversion into CO and O₂

$$E_F = \Delta G^\ominus * M_{CO} = 2.57 * 10^5 * M_{CO} \text{ J}$$

Table S1 LTCO conversion efficiency calculation data.

light	sample	M_{CO} (μ mol)	E_F (J)	E_{light} (J)	LTCO (10^{-6})
UV-Vis	BOC-OV	0.844	0.217	8208	26.5
	BOC	0.2945	0.0755		9

1.5 Photoelectrochemical measurements

Transient photocurrent response and electrochemical impedance of the samples were measured in a three-electrode quartz cell containing Na_2SO_4 (0.1 M) electrolyte solution and using a CHI630E electrochemical working station (CHI Instruments, Shanghai, China). Samples were located on a fluorinated-tin-oxide (FTO) conducting glass as the working electrode. Ag/AgCl and Pt played the role of reference and counter electrodes, respectively.

1.6 In-situ DRIFTS measurement

During the in-situ DRIFTS measurement, the sample was filled into the in-situ IR cell, and CO_2 and H_2O gases were introduced into the cell and LED monochromatic light of 365 nm irradiated on the sample through the CaF_2 window of the cell. Before the measurement, the sample was degassed at 423 K for 4 h. The baseline was obtained after adsorption equilibrium of CO_2 on the sample for 1 h.

2 Theoretical calculations

The first-principles density functional theory plus dispersion method implemented in the DMol³ package was used for all the calculations of the study.[1,2] All the structures are fully optimized using the generalized gradient approximation (GGA), treated by the Perdew–Burke–Ernzerhof exchange–correlation potential (PBE) with long range dispersion correction via TS’s scheme.[3] An all electron double numerical atomic orbital augmented by d-polarization functions (DNPs) is used as the basis set. The vacuum between the BiOCl monolayers is 15 Å which is large enough to avoid interactions between periodic images. Geometry optimizations were performed with convergence thresholds of 0.004 ha Å⁻¹ on the gradient, 0.005 Å on the displacement, and 2×10^{-5} ha on the energy. The self-consistent field (SCF) procedure was used with a 1.0^{-5} ha value. The Brillouin zones are sampled by $5 \times 5 \times$

1k-points using the Monkhorst–Pack scheme.[4] The bulk structure of BiOCl belongs to the tetragonal space group P4/nmm (NO 129).[5] The optimized lattice constant of the BiOCl monolayer is 3.89 Å, and a 3 × 3 supercell of the BiOCl (001) monolayer with a dimension of 11.67 × 11.67 × 22.37 Å³ was used for CO₂ reduction. Meanwhile, to investigate the effect of oxygen vacancy for BiOCl, one of oxygen atoms was removed to build up possible oxygen vacancy in the BiOCl system. The LST/QST tools were employed to calculate the activation barrier energies (E_a) and transition states (TS) of CO₂ reduction paths.[6]

- (1). B. Delley, An all-electron numerical method for solving the local density functional for polyatomic molecules, *J. Chem. Phys.*, 1990,92, 508-517;
- (2). B. Delley, From molecules to solids with the DMol3 approach, *J. Chem. Phys.*, 2000,113, 7756-7764.
- (3). J. P. Perdew, K. Burke, M. Ernzerhof, Generalized Gradient Approximation Made Simple, *Phys. Rev. Lett.*, 1996,77 (18), 3865-3868.
- (4). D. J. Chadi, M. L. Cohen, Special Points in the Brillouin Zone, *Phys. Rev. B*, 1973,8, 5747-5753.
- (5). R. W. G. Wyckoff, *Crystal Structures*, second ed., vol. 1, Wiley, New York, 1963
- (6). T. A. Halgren, W. N. Lipscomb, The synchronous-transit method for determining reaction pathways and locating molecular transition states, *Chem. Phys. Lett.*, 1977,49, 225-232.

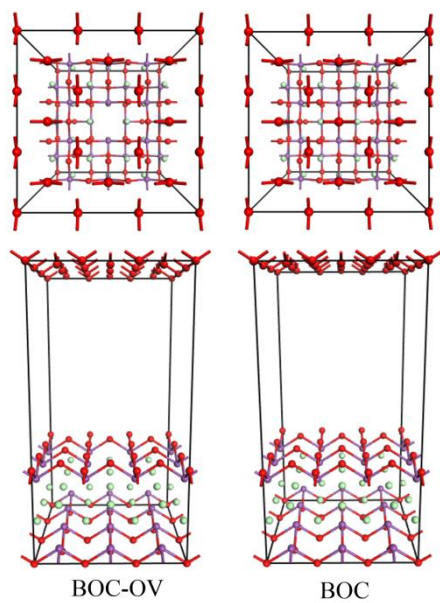


Figure S1 Atomic structure of BOC-OV and BOC.

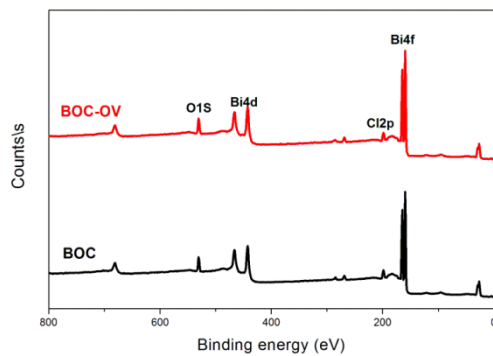


Figure S2 XPS of BOC-OV and BOC.

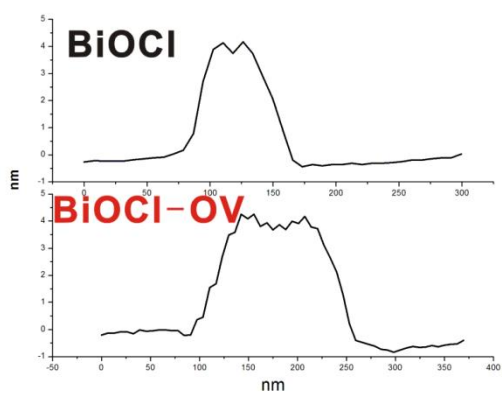
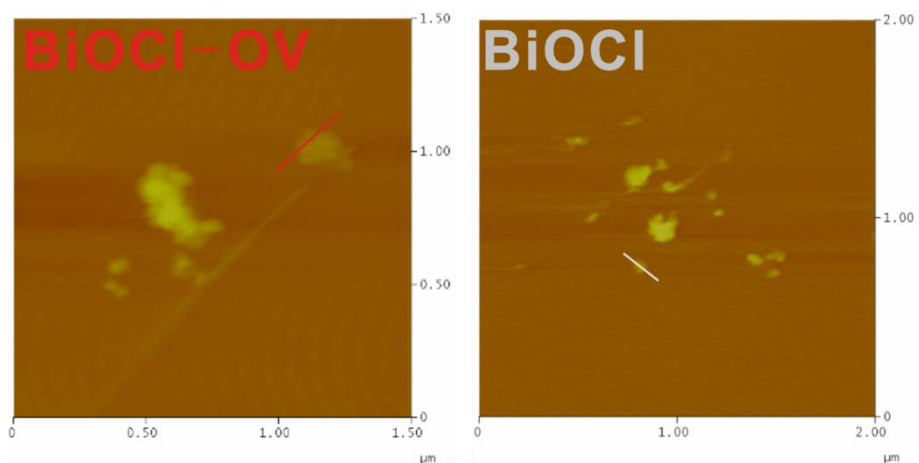


Figure S3 AFM image of BOC-OV and BOC.

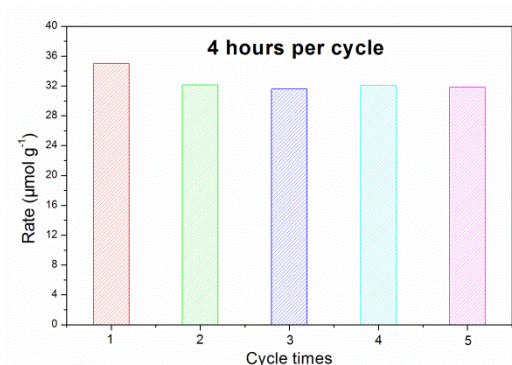


Figure S4 Cycling test of photocatalytic CO_2 reduction on BOC-OV.

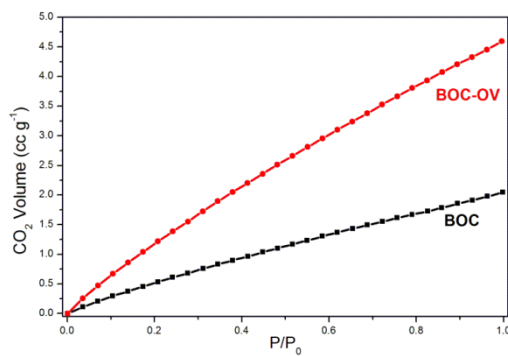


Figure S5 CO_2 adsorption performance of BOC-OV and BOC.

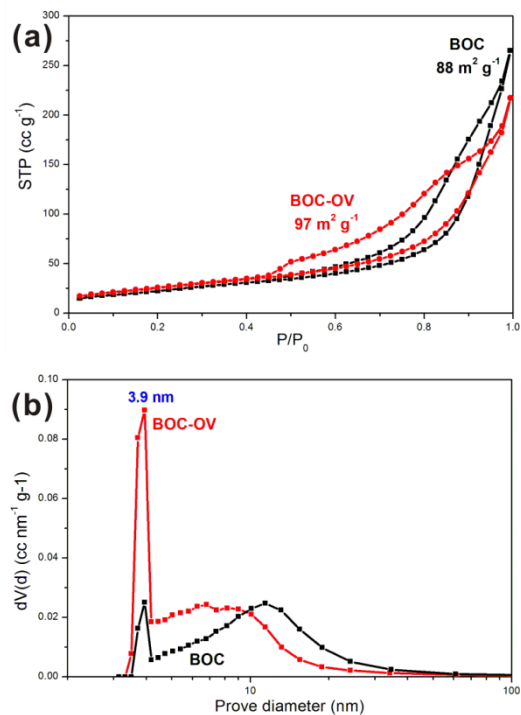


Figure S6 (a) Nitrogen adsorption–desorption isotherms and (b) corresponding pore size distribution curves of BOC-OV and BOC.

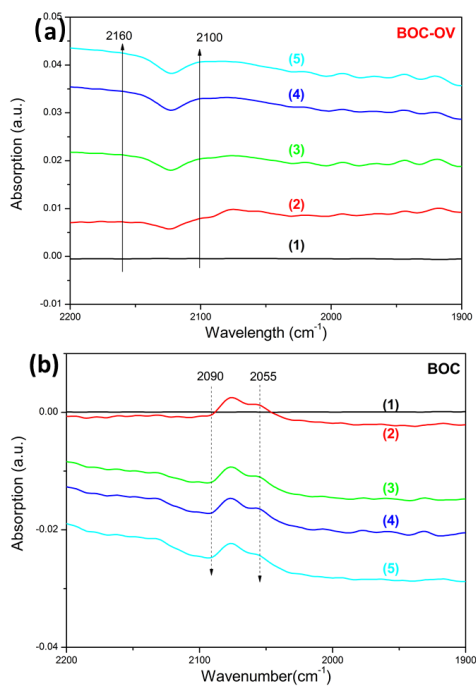


Figure S7 In-situ DRIFT spectra of CO₂ reduction on BOC-OV (a) and BOC (b).

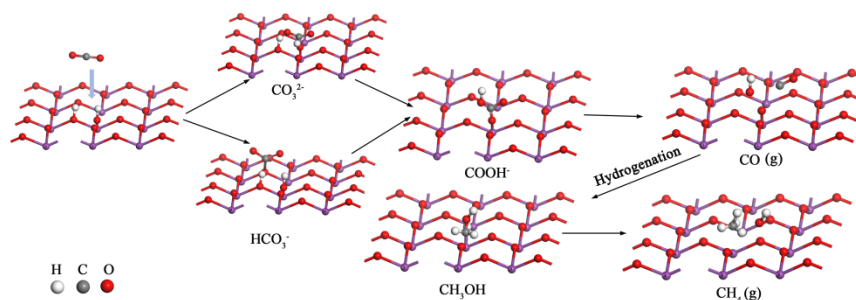


Figure S8 Possible schematic mechanisms for CO₂ reduction on BOC-OV.

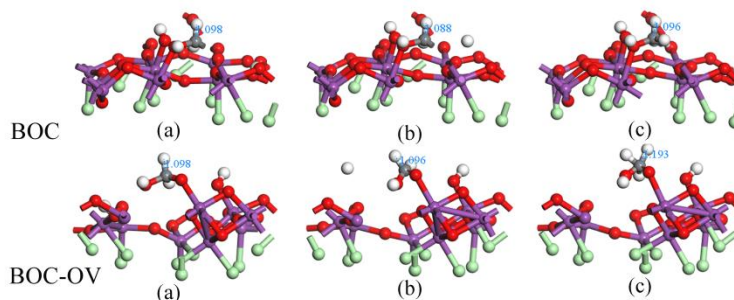


Figure S9 The optimized geometries of CH₂OH* hydrogenation to CH₃OH*: reactant (a), transition state (b) and product (c).

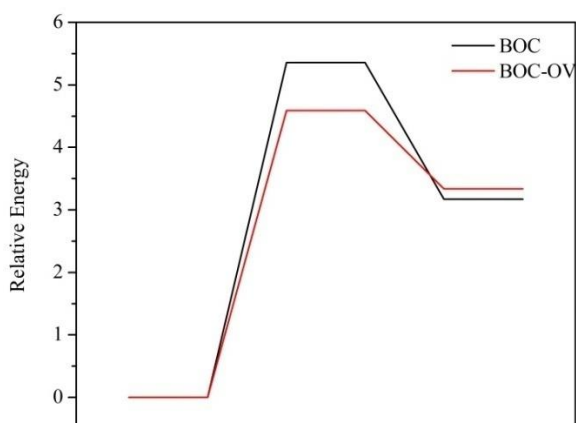


Figure S10 Potential energy profiles of the direct dissociation of CO₂ to CO.

Table S2 Assigned surface species of observed wavenumbers on BOC-OV and BOC.

species	Assignment	Wavenumber (cm ⁻¹)		Ref.
		BOC-OV	BOC	
Terminal-OH	-OH	3729/3702/ 3626/3599	3729/3702/ 3626/3599	3800-3600 ^{1,2}
CO ₂		2360/2337	2360/2337	2361 ³
Bidentate carbonate	v(CO)	1058		1059 ⁴
Carbonate	v _{as} (CO ₃)	1318/1058	1314/1309	1321 ⁴ /1315 ⁵ / 1055 ⁴
Bicarbonate		1645/1480/ 1437	1645	1645 ⁶ /1481 ⁴ / 1438 ⁶

Bidentateformate	$\delta(\text{CH}) + \nu_{\text{as}}(\text{OCO})$		2963	2965 ⁷ ,2967 ⁸
	$\nu(\text{CH})$	2872		2872 ⁷ ,2880 ⁸
Formate	$\nu_{\text{as}}(\text{OCO})$	1558	1561	1570-1560 ⁹
	$\nu(\text{CO})$		1698	1698-1701 ¹⁰
CH ₃ OH	$\nu(\text{CH}_3)$		2851/2923	2954 ¹¹ /2849 ⁷
CH ₃ OH			1029	1030 ¹²
Methoxy	$\nu(\text{CO})$	1124		1124 ⁷

- (1) B. Bachiller-Baeza, I. Rodriguez-Ramos, A. Guerrero-Ruiz, Interaction of Carbon Dioxide with the Surface of Zirconia Polymorphs, *Langmuir*, 1998, 14, 3556-3564.
- (2) A. A. Tsyganenko, V. N. Filimonov, Infrared Spectra of Surface Hydroxyl Groups and Crystalline Structure of Oxides, *Spectroscopy Lett.*, 1972, 5, 477-487.
- (3) L. F. Liotta, G. A. Martin, G. Deganello, The Influence of Alkali Metal Ions in the Chemisorption of CO and CO₂ on Supported Palladium Catalysts: A Fourier Transform Infrared Spectroscopic Study, *J.Catal.*, 1996, 164, 322-333.
- (4) W. Wu, K. Bhattacharyya, K. Gray, E. Weitz, Photoinduced Reactions of Surface-Bound Species on Titania Nanotubes and Platinized Titania Nanotubes: An in Situ FTIR Study, *J. Phys. Chem. C*, 2013, 117, 20643-20655.
- (5) M.-T. Chen, C.-F. Lien, L.-F. Liao; J.-L. Lin, In-Situ FTIR Study of Adsorption and Photoreactions of CH₂Cl₂ on Powdered TiO₂, *J. Phys. Chem. B*, 2003, 107, 3837-3843.
- (6) J. Szanyi, J. H. Kwak, Dissecting the steps of CO₂ reduction: 1. The interaction of CO and CO₂ with $[\gamma]\text{-Al}_2\text{O}_3$: an in situ FTIR study, *Phys. Chem. Chem. Phys.*, 2014, 16, 15117-15125.
- (7) S. Kattel, B. Yan, Y. Yang, J. G. Chen, P. Liu, Optimizing Binding Energies of Key Intermediates for CO₂ Hydrogenation to Methanol over Oxide-Supported Copper, *J. Am. Chem. Soc.*, 2016, 138, 12440-12450.
- (8) D. Bianchi, T. Chafik, M. Khalfallah, S. J. Teichner, Intermediate species on zirconia supported methanol aerogel catalysts, *Appl. Catal. A: Gen.*, 1993, 105, 223-249.
- (9) P. O. Graf, D. J. M. de Vlieger, B. L. Mojet, L. Lefferts, New insights in reactivity of hydroxyl groups in water gas shift reaction on Pt/ZrO₂, *J. Catal.*, 2009, 262, 181-187.
- (10) M. El-Maazawi, A. N. Finken, A. B. Nair, V. H. Grassian, Adsorption and Photocatalytic Oxidation of Acetone on TiO₂: An in Situ Transmission FT-IR Study, *J. Catal.*, 2000, 191, 138-146.

(11) J. Szanyi, J. H. Kwak, Photo-catalytic oxidation of acetone on a TiO₂ powder: An in situ FTIR investigation, *J. Mol. Catal. A: Chem.*, 2015, 406, 213-223.

(12) M. Manzoli, A. Chiorino, F. Boccuzzi, Decomposition and combined reforming of methanol to hydrogen: a FTIR and QMS study on Cu and Au catalysts supported on ZnO and TiO₂, *Appl. Catal. B: Environ.*, 2005, 57, 201-209.